




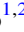




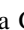
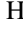











# The Curious Case of PHL 293B: A Long-lived Transient in a Metal-poor Blue Compact Dwarf Galaxy

Colin J. Burke<sup>1,2</sup> , Vivienne F. Baldassare<sup>3,42</sup> , Xin Liu<sup>1,2</sup> , Ryan J. Foley<sup>4</sup>, Yue Shen<sup>1,2,43</sup> , Antonella Palmese<sup>5,6</sup> , Hengxiao Guo<sup>1,2</sup> , Kenneth Herner<sup>5</sup>, Tim M. C. Abbott<sup>7</sup>, Michel Aguena<sup>8,9</sup>, Sahar Allam<sup>5</sup>, Santiago Avila<sup>10</sup>, Emmanuel Bertin<sup>11,12</sup>, David Brooks<sup>13</sup> , Aurelio Carnero Rosell<sup>14</sup>, Matias Carrasco Kind<sup>1,2</sup> , Jorge Carretero<sup>15</sup>, Luiz N. da Costa<sup>9,16</sup>, Juan De Vicente<sup>14</sup>, Shantanu Desai<sup>17</sup>, Peter Doel<sup>13</sup>, Tim F. Eifler<sup>18,19</sup>, Spencer Everett<sup>20</sup>, Josh Frieman<sup>5,21</sup>, Juan García-Bellido<sup>10</sup> , Enrique Gaztanaga<sup>22,23</sup>, Daniel Gruen<sup>24,25,26</sup> , Robert A. Gruendl<sup>1,2</sup> , Julia Gschwend<sup>9,16</sup>, Gaston Gutierrez<sup>5</sup>, Devon L. Hollowood<sup>20</sup> , Klaus Honscheid<sup>27,28</sup>, David J. James<sup>29</sup>, Elisabeth Krause<sup>18</sup>, Kyler Kuehn<sup>30,31</sup> , Marcio A. G. Maia<sup>9,16</sup>, Felipe Menanteau<sup>1,2</sup>, Ramon Miquel<sup>15,32</sup> , Francisco Paz-Chinchón<sup>22,33</sup>, Andrés A. Plazas<sup>34</sup>, Eusebio Sanchez<sup>14</sup> , Basilio Santiago<sup>9,35</sup>, Vic Scarpine<sup>5</sup>, Santiago Serrano<sup>22,23</sup>, Ignacio Sevilla-Noarbe<sup>14</sup>, Mathew Smith<sup>36</sup>, Marcelle Soares-Santos<sup>37</sup> , Eric Suchyta<sup>38</sup>, Molly E. C. Swanson<sup>2</sup> , Gregory Tarle<sup>39</sup> , Douglas L. Tucker<sup>5</sup>, Tamas Norbert Varga<sup>40,41</sup>, and Alistair R. Walker<sup>7</sup> 

(DES Collaboration)

<sup>1</sup> Department of Astronomy, University of Illinois at Urbana-Champaign, 1002 W. Green Street, Urbana, IL 61801, USA; [colinj2@illinois.edu](mailto:colinj2@illinois.edu)

<sup>2</sup> National Center for Supercomputing Applications, 1205 West Clark Street, Urbana, IL 61801, USA

<sup>3</sup> Department of Astronomy, Yale University, 52 Hillhouse Avenue, New Haven, CT 06511, USA

<sup>4</sup> Department of Astronomy and Astrophysics, University of California, Santa Cruz, CA 95064, USA

<sup>5</sup> Fermi National Accelerator Laboratory, P.O. Box 500, Batavia, IL 60510, USA

<sup>6</sup> Kavli Institute for Cosmological Physics, University of Chicago, 5640 South Ellis Avenue, Chicago, IL 60637, USA

<sup>7</sup> Cerro Tololo Inter-American Observatory, NSF's National Optical-Infrared Astronomy Research Laboratory, Casilla 603, La Serena, Chile

<sup>8</sup> Departamento de Física Matemática, Instituto de Física, Universidade de São Paulo, CP 66318, São Paulo, SP, 05314-970, Brazil

<sup>9</sup> Laboratório Interinstitucional de e-Astronomia—LIneA, Rua Gal. José Cristino 77, Rio de Janeiro, RJ—20921-400, Brazil

<sup>10</sup> Instituto de Física Teórica UAM/CSIC, Universidad Autónoma de Madrid, E-28049 Madrid, Spain

<sup>11</sup> CNRS, UMR 7095, Institut d'Astrophysique de Paris, F-75014, Paris, France

<sup>12</sup> Sorbonne Universités, UPMC Univ. Paris 06, UMR 7095, Institut d'Astrophysique de Paris, F-75014, Paris, France

<sup>13</sup> Department of Physics & Astronomy, University College London, Gower Street, London, WC1E 6BT, UK

<sup>14</sup> Centro de Investigaciones Energéticas, Medioambientales y Tecnológicas (CIEMAT), Madrid, Spain

<sup>15</sup> Institut de Física d'Altes Energies (IFAE), The Barcelona Institute of Science and Technology, Campus UAB, E-08193 Bellaterra (Barcelona) Spain

<sup>16</sup> Observatório Nacional, Rua Gal. José Cristino 77, Rio de Janeiro, RJ—20921-400, Brazil

<sup>17</sup> Department of Physics, IIT Hyderabad, Kandi, Telangana 502285, India

<sup>18</sup> Department of Astronomy/Steward Observatory, University of Arizona, 933 North Cherry Avenue, Tucson, AZ 85721-0065, USA

<sup>19</sup> Jet Propulsion Laboratory, California Institute of Technology, 4800 Oak Grove Drive, Pasadena, CA 91109, USA

<sup>20</sup> Santa Cruz Institute for Particle Physics, Santa Cruz, CA 95064, USA

<sup>21</sup> Kavli Institute for Cosmological Physics, University of Chicago, Chicago, IL 60637, USA

<sup>22</sup> Institut d'Estudis Espacials de Catalunya (IEEC), E-08034 Barcelona, Spain

<sup>23</sup> Institute of Space Sciences (ICE, CSIC), Campus UAB, Carrer de Can Magrans, s/n, E-08193 Barcelona, Spain

<sup>24</sup> Department of Physics, Stanford University, 382 Via Pueblo Mall, Stanford, CA 94305, USA

<sup>25</sup> Kavli Institute for Particle Astrophysics & Cosmology, P.O. Box 2450, Stanford University, Stanford, CA 94305, USA

<sup>26</sup> SLAC National Accelerator Laboratory, Menlo Park, CA 94025, USA

<sup>27</sup> Center for Cosmology and Astro-Particle Physics, The Ohio State University, Columbus, OH 43210, USA

<sup>28</sup> Department of Physics, The Ohio State University, Columbus, OH 43210, USA

<sup>29</sup> Center for Astrophysics | Harvard & Smithsonian, 60 Garden Street, Cambridge, MA 02138, USA

<sup>30</sup> Australian Astronomical Optics, Macquarie University, North Ryde, NSW 2113, Australia

<sup>31</sup> Lowell Observatory, 1400 Mars Hill Road, Flagstaff, AZ 86001, USA

<sup>32</sup> Institució Catalana de Recerca i Estudis Avançats, E-08010 Barcelona, Spain

<sup>33</sup> Institute of Astronomy, University of Cambridge, Madingley Road, Cambridge CB3 0HA, UK

<sup>34</sup> Department of Astrophysical Sciences, Princeton University, Peyton Hall, Princeton, NJ 08544, USA

<sup>35</sup> Instituto de Física, UFRGS, Caixa Postal 15051, Porto Alegre, RS—91501-970, Brazil

<sup>36</sup> School of Physics and Astronomy, University of Southampton, Southampton, SO17 1BJ, UK

<sup>37</sup> Brandeis University, Physics Department, 415 South Street, Waltham MA 02453, USA

<sup>38</sup> Computer Science and Mathematics Division, Oak Ridge National Laboratory, Oak Ridge, TN 37831, USA

<sup>39</sup> Department of Physics, University of Michigan, Ann Arbor, MI 48109, USA

<sup>40</sup> Max Planck Institute for Extraterrestrial Physics, Giessenbachstrasse, D-85748 Garching, Germany

<sup>41</sup> Universitäts-Sternwarte, Fakultät für Physik, Ludwig-Maximilians Universität München, Scheinerstr. 1, D-81679 München, Germany

Received 2020 February 27; revised 2020 April 11; accepted 2020 April 14; published 2020 April 29

## Abstract

We report on small-amplitude optical variability and recent dissipation of the unusually persistent broad emission lines in the blue compact dwarf galaxy PHL 293B. The galaxy's unusual spectral features (P Cygni-like profiles with  $\sim 800 \text{ km s}^{-1}$  blueshifted absorption lines) have resulted in conflicting interpretations of the nature of this source in the literature. However, analysis of new Gemini spectroscopy reveals the broad emission has begun to fade after

<sup>42</sup> Einstein Fellow.

<sup>43</sup> Alfred P. Sloan Fellow.

being persistent for over a decade prior. Precise difference imaging light curves constructed with the Sloan Digital Sky Survey and the Dark Energy Survey reveal small-amplitude optical variability of  $\sim 0.1$  mag in the  $g$  band offset by  $100 \pm 21$  pc from the brightest pixel of the host. The light curve is well-described by an active galactic nuclei (AGN)-like damped random walk process. However, we conclude that the origin of the optical variability and spectral features of PHL 293B is due to a long-lived stellar transient, likely a Type II<sub>n</sub> supernova or nonterminal outburst, mimicking long-term AGN-like variability. This work highlights the challenges of discriminating between scenarios in such extreme environments, relevant to searches for AGNs in dwarf galaxies. This is the second long-lived transient discovered in a blue compact dwarf, after SDSS1133. Our result implies such long-lived stellar transients may be more common in metal-deficient galaxies. Systematic searches for low-level variability in dwarf galaxies will be possible with the upcoming Legacy Survey of Space and Time at the Vera C. Rubin Observatory.

*Unified Astronomy Thesaurus concepts:* Type II supernovae (1731); Transient detection (1957); Luminous blue variable stars (944); Blue compact dwarf galaxies (165); Dwarf galaxies (416); Galaxies (573)

## 1. Introduction

Blue compact dwarf (BCD) galaxies (Thuan & Martin 1981), particularly metal-poor ones, are important laboratories for studying galaxies in their earliest stages of evolution. They may be undergoing their first round of star formation, containing massive O and B stars responsible for their blue colors. Therefore, BCD galaxies may act as analogs to primordial high redshift galaxies, offering unique opportunities to study intense star formation and low-metallicity environments.

PHL 293B<sup>44</sup> is a metal-poor ( $12 + \log O/H = 7.71 \pm 0.02$ ; Izotov et al. 2011) BCD emission-line galaxy at  $z = 0.00517 \pm 0.00001$  (NED).<sup>45</sup> PHL 293B has a stellar mass of  $\sim 2 \times 10^7 M_{\odot}$  and an H I gas fraction of 0.75 (Geha et al. 2006). The source previously exhibited striking P Cygni-like broad emission in Balmer series lines (Izotov & Thuan 2009a; Izotov et al. 2011). The narrow absorption lines were blueshifted by  $\sim 800$  km s<sup>-1</sup> and the broad H $\alpha$  emission had an FWHM of about 1500 km s<sup>-1</sup>. The spectral features (including broad lines) persisted for over a decade until only recently. The origin of these features has been a source of speculation, with conflicting interpretations in the literature. A luminous blue variable (LBV) star outburst (Izotov & Thuan 2009a; Izotov et al. 2011; Allan et al. 2020), an expanding supershell or stationary superwind driven by a young stellar wind (Terlevich et al. 2014), and a strongly radiative stationary cooling wind driven by old supernova remnants (Tenorio-Tagle et al. 2015) have been proposed.

Here we report on variability measured in the optical light curves using difference imaging on Sloan Digital Sky Survey (SDSS) and years 1–6 (Y6) Dark Energy Survey (DES; Flaugher et al. 2015; Dark Energy Survey Collaboration 2016; Drlica-Wagner et al. 2018) images. The previously undetected variability has an amplitude of 0.12 mag in the  $g$  band between 1998 and 2018. This observation rules out stationary winds and other nontransient interpretations for the mechanism of the broad emission lines in PHL 293B. The optical variability is well-described by a damped random walk process typical of active galactic nuclei (AGN; Kelly et al. 2009; MacLeod et al. 2010). However, analysis of recently obtained Gemini GMOS-N spectroscopy reveals the broad emission component has now begun to subside. A changing-look AGN scenario is unlikely given the lack of X-ray emission and high-ionization lines, as

discussed in Section 3.2. Most likely, the variability is due to a transient event mimicking AGN-like variability.

In light of our new observations, we investigate several scenarios that could explain the features of PHL 293B. We conclude that the source of the variability and spectral features of PHL 293B is most likely due to a long-lived Type II<sub>n</sub> supernova (SN II<sub>n</sub>)-like transient. In particular, we speculate that we could be observing a similar event to the peculiar long-lived transient SDSS J113323.97+550415.8 (SDSS1133) in the BCD galaxy Mrk 177 discovered by Koss et al. (2014). In this scenario, an LBV progenitor explodes as an SN II<sub>n</sub>-like event, followed by a slowly flattening light curve and unusually persistent broad emission-line features.

This Letter is organized as follows. In Section 2, we present combined SDSS and DES light curves, which show a slowly fading transient, along with new Gemini GMOS-N spectroscopy, which shows that the broad emission has recently faded. In Section 3.1, we summarize the existing observations of PHL 293B in the literature. In Section 3.2, we review the interpretations of the nature of PHL 293B in the literature and attempt to reconcile its newly observed photometric and spectroscopic variability with the previous work. In Section 4, we summarize our findings and conclude that, contrary to previous explanations, PHL 293B is most likely a long-lived SN II<sub>n</sub>-like event.

## 2. New Observations

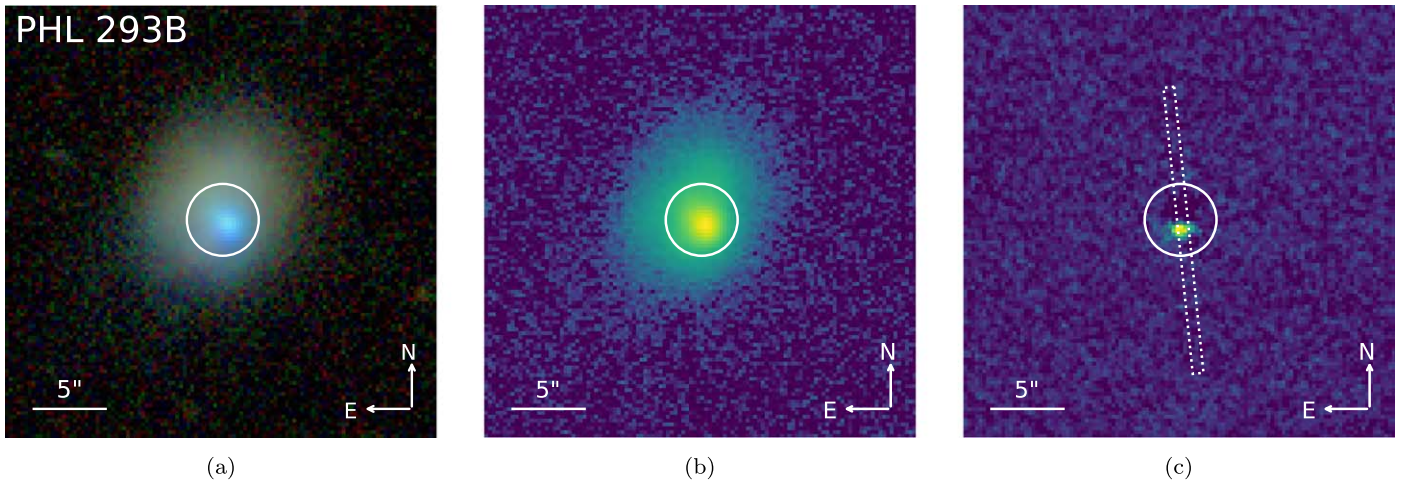
### 2.1. SDSS+DES Light Curve

The optical variability in PHL 298B was discovered independently in searches for AGN in dwarf galaxies in SDSS (Baldassare et al. 2018) and in DES (Burke et al. in preparation). Here, we combine the SDSS and DES light curves for a total baseline spanning two decades (1998–2018). We perform standard difference image analysis (DIA) to isolate the variable point-source flux from seeing variations between epochs.

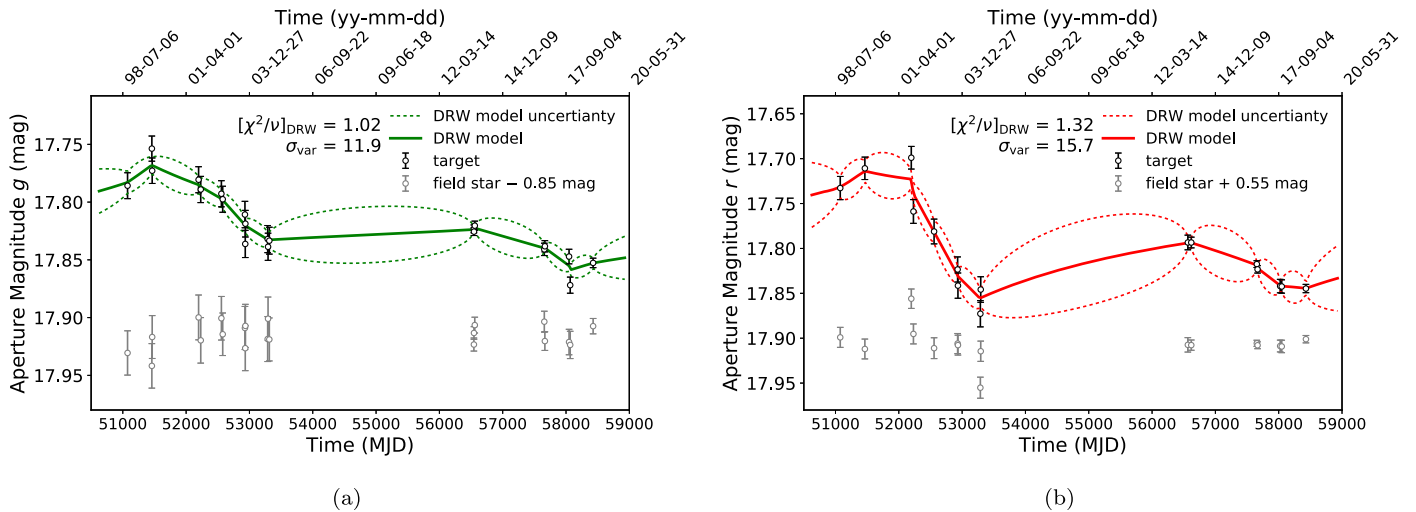
We summarize the analysis and features of the light curve here; see Appendix A for details. The DES coadd, template image, difference image coadd, and the DIA multiband SDSS+DES light curves are shown in Figure 1. The difference image flux is consistent with an unresolved point-source offset by  $3.5 \pm 0.7$  pixels or  $100 \pm 21$  pc from the brightest pixel of the host. The SDSS photometry was taken between MJD 51075 and 53314 (between 1998 and 2005). The DES photometry was taken between MJD 56545 and 58428 (between 2013 and 2018). The amplitude is 0.12 mag ( $g$  band) which corresponds to an  $\sim 10\%$  variation in luminosity over 20 yr.

<sup>44</sup> Also known as the Kinman dwarf or SDSS J223036.79-000636.9.

<sup>45</sup> For consistency with Terlevich et al. (2014), a distance of 23.1 Mpc is adopted throughout (corrected for the Virgo cluster + Great Attractor + Shapley) using  $H_0 = 73.0$  km s<sup>-1</sup> Mpc<sup>-1</sup>,  $\Omega_m = 0.27$ , and  $\Omega_{\Lambda} = 0.73$ . See [http://ned.ipac.caltech.edu/byname?objname=kinman%20dwarf&hconst=73.0&omegam=0.27&omegav=0.73&wmap=1&corr\\_z=4](http://ned.ipac.caltech.edu/byname?objname=kinman%20dwarf&hconst=73.0&omegam=0.27&omegav=0.73&wmap=1&corr_z=4).



**Figure 1.** Difference imaging analysis of PHL 293B photometry with SDSS and DES. The top row shows (a) the DES *gri* color composite Y6 coadd, (b) the DES *g* band template image, and (c) the DES *g* band coadd of the difference images. The circles enclose the  $2''.5$  radius target aperture. The GMOS slit configuration is also shown in panel (c). The difference images indicate a single variable point-source offset by  $100 \pm 21$  pc.



**Figure 2.** SDSS and DES combined difference imaging light curves of PHL 293B (target) are shown in *g* (a) and *r* (b) bands. A nearby field star is shown for comparison. The best-fit damped random walk (DRW) model (solid lines) and model uncertainty (dashed lines) are shown. The light curves are constructed from SDSS and DES imaging between 1998 and 2018.

We originally selected PHL 293B as having variability consistent with an AGN. To test this in more detail, we fit the light curve to a damped random walk (DRW) model (generally a good empirical descriptor of AGN variability on timescales of days to years; Kelly et al. 2009; MacLeod et al. 2010). To assess the fit, we calculate the reduced  $\chi^2$  of the DRW model  $[\chi^2/\nu]_{\text{DRW}}$ . We also calculate the significance that the source is variable  $\sigma_{\text{var}}$  in units of  $\sigma$  from a  $\chi^2$  test given the photometry and uncertainties (see Appendix A). We find the *g*-band variability is significant at the  $11\sigma$  level, and the DRW model is a good fit to the data. However, the overall trend is a slow fading at a rate of  $\sim 0.005$  mag  $\text{year}^{-1}$  in the *g* band. Along with the evidence presented in Section 3.2, we conclude that we are instead witnessing a long-lived transient mimicking AGN-like variability.

The nearby field star J223033.18-000633.7 is used for comparison and to correct for any zero-point difference between the SDSS and DES photometric systems. The field star is not significantly variable (*g*-band  $\sigma_{\text{var}} = 0.16$ ). The variability of PHL 293B is marginally significant in the DES data and certainly present in SDSS. Inspection of the difference

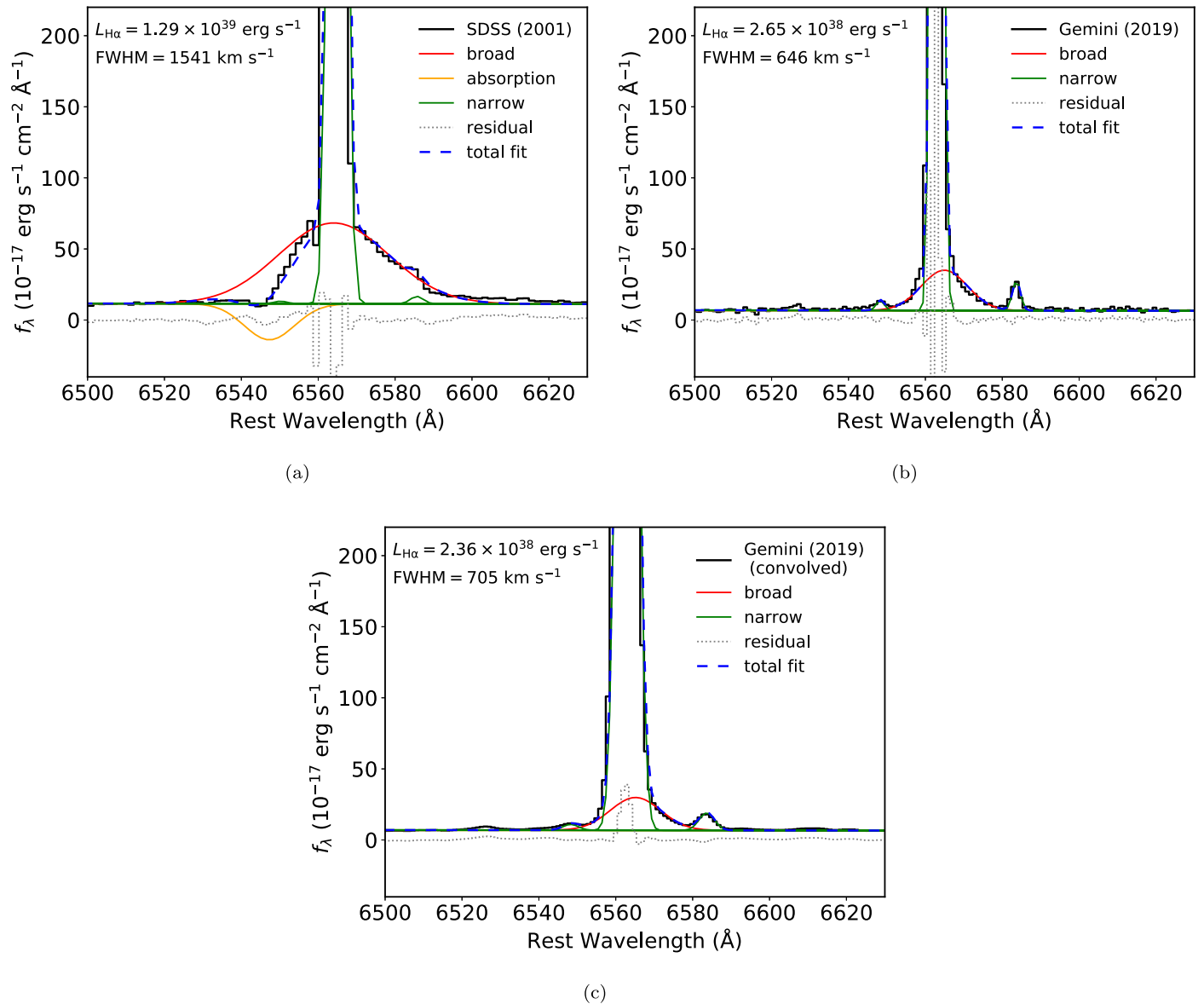
images by eye did not reveal any artifacts that would indicate a bad image subtraction. Furthermore, the same variable trend is present in all photometric bands, indicating it is not due to a systematic (Figure 2).

## 2.2. Gemini Spectroscopy

Gemini Director’s Time observations of PHL 293B (GN-2019B-DD-109, P.I. Baldassare) were taken on 2019 December 20. Spectra were taken using the Gemini Multi Object Spectrograph (GMOS) on Gemini North. We used the  $0''.75$  slit with the R831\_G5302 grating, yielding a spectral resolution of  $R \approx 4500$ . The central wavelength was set to 6600 Å, giving wavelength coverage from 5500 to 7500 Å. The seeing was  $0''.65$ .

Spectra were reduced following the steps laid out in the GMOS Cookbook for the reduction of long-slit spectra with PyRAF.<sup>46</sup> These include bias subtraction, flat-field correction, wavelength calibration, cosmic-ray rejection, and flux

<sup>46</sup> [http://ast.noao.edu/sites/default/files/GMOS\\_Cookbook/](http://ast.noao.edu/sites/default/files/GMOS_Cookbook/)



**Figure 3.**  $H\alpha$ -[N II] complex from the SDSS (a) and Gemini (b) spectrum of PHL 293B. We convolved the Gemini spectrum with a Gaussian of width  $\text{FWHM} = 1541 \text{ km s}^{-1}$  to match the GMOS spectral resolution to SDSS. This is shown in panel (c) to facilitate comparison (assuming the narrow  $H\alpha$  emission is unchanged). The data is shown in black and the best-fit model is overplotted in blue. The individual components—narrow lines, broad line, and absorption—are plotted in green, red, and orange, respectively. The reported FWHM and luminosity refer to the broad emission component shown in red. The uncertainties are dominated by systematics.

calibration using the flux standard. The Gaussian spectral fitting is shown in Figure 3, and was done with the PYQSOFIT code (Guo et al. 2018; Shen et al. 2019). We fit a continuum and Gaussian emission/absorption lines within user-defined windows and constraints on their widths. The continuum is modeled as a blue power-law plus a third-order polynomial for reddening. The total model is a linear combination of the continuum and single or multiple Gaussians for the emission lines. Since uncertainties in the continuum model may induce subtle effects on measurements for weak emission lines, we first perform a global fit to the emission-line free region to better quantify the continuum.

We then fit multiple Gaussian models to the continuum-subtracted spectrum around the  $H\alpha$  emission-line region locally. For the SDSS  $H\alpha$ , we fit three Gaussians to model the narrow emission, broad emission, and absorption line. We use one narrow and one broad Gaussian to model the Gemini

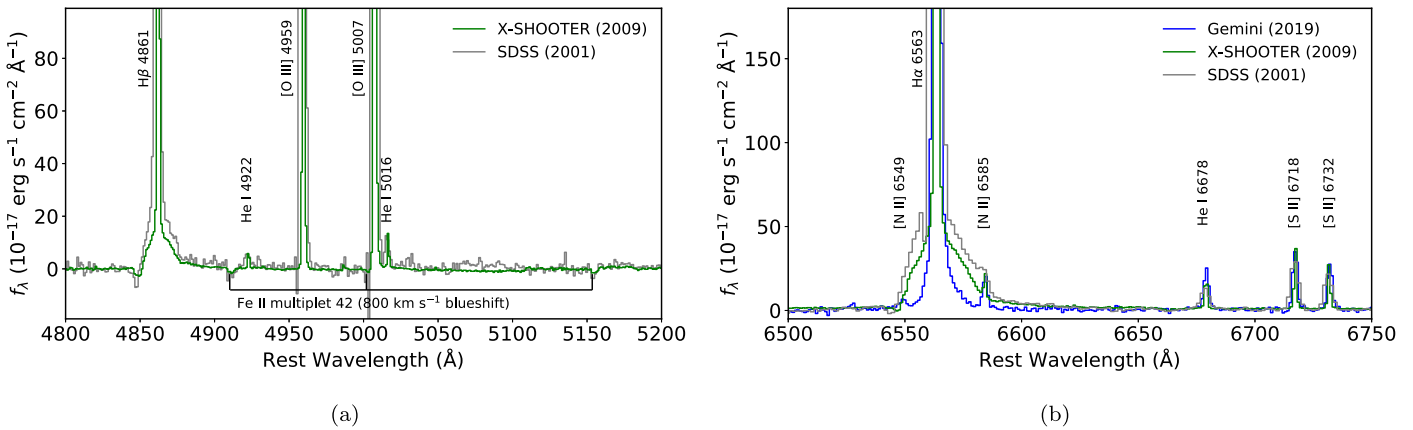
$H\alpha$  emission. Narrow Gaussians are defined as having  $\text{FWHM} < 500 \text{ km s}^{-1}$ . The narrow and broad line centroids are fit within a window of  $\pm 65 \text{ \AA}$  and  $\pm 100 \text{ \AA}$ , respectively. We use 100 Monte Carlo simulations to estimate the uncertainty in the line measurements. The spectral fitting of the  $H\alpha$ -[N II] complex is shown in Figure 3 along with the SDSS spectral epoch taken in 2001 for comparison.

### 3. Discussion

#### 3.1. Comparison with Existing Observations

##### 3.1.1. Photometry

The earliest photometry for PHL 293B is reported in Kinman (1965) from the Palomar Sky Survey in 1965 and the Lick Observatory Carnegie Astrograph in 1949. Kinman (1965) writes, “a very rough estimate of the  $B$  magnitude is 17.7 on the



**Figure 4.** Comparison of the SDSS, X-SHOOTER (Izotov et al. 2011), and Gemini GMOS-N spectra near  $H\beta$  (a) and  $H\alpha$  (b). All spectra are binned to  $\Delta\log\lambda = 10^{-4}$ , flux-calibrated, dereddened, redshift-corrected, and continuum model-subtracted. Differences between the SDSS and X-SHOOTER spectra can be attributed to aperture effects. The P Cygni-like absorption features are clearly present in the X-SHOOTER ( $1''$  slit width) and SDSS ( $3''$  fiber) data. The Gemini spectrum clearly shows the broad emission has begun to fade and the absorption feature is gone.

Sky Survey plates and about a half-magnitude fainter on the 120-inch plates.” Cairós et al. (2001) report a  $B$  magnitude of 17.67 in 1988 October. The source is no brighter in the infrared than our comparison field star in digitized Sky Survey data taken on 1995 September.

The galaxy’s morphology was studied by Tarrab (1987). Later, the light profile was studied in more detail by Micheva et al. (2013), who obtained deep multiband imaging using the Nordic Optical Telescope in 2001. Micheva et al. (2013) report a  $B$  magnitude of 17.3. However, this difference can perhaps be attributed to instrument errors and different aperture definitions.

Catalina Sky Survey (CSS) photometry is available between 2005 April and 2013 October (roughly in-between the SDSS and DES photometry) and is analyzed in Terlevich et al. (2014). However, the scatter in the CSS photometry is  $\sim 0.1$   $V$  mag. Still, we can rule out any large variability greater than one-tenth of a magnitude in-between the SDSS and DES observations shown in Figure 2. Our SDSS+DES light curve is consistent with Terlevich et al. (2014), who constrain any variability over a few years to less than 0.02 mag and over 25 yr to less than a few tenths of magnitude. There is a gap in the photometry between 1995 September and the beginning of the SDSS data in 1998 September.

The lack of large photometric variability and lack of spectral variability seen in PHL 293B prior to this work resulted in Terlevich et al. (2014) and Tenorio-Tagle et al. (2015) concluding that the source is not transient in nature. Given the small-amplitude optical variability from our precise DIA photometry and the recent dissipation of the unusually persistent broad  $H\alpha$  emission, it is now clear that this is not the case. A complete reinterpretation of PHL 293B is now warranted.

### 3.1.2. Spectroscopy

The earliest spectrum of PHL 293B is shown in Kinman (1965). The presence of any broad emission is difficult to distinguish from the noise considering the [O III]  $\lambda 4363$  line is barely detected in their spectrum. Later, French (1980) studied the line fluxes and its chemical abundance.

In 2001, PHL 293B was observed spectroscopically with SDSS. Broad and narrow Balmer emission with P Cygni profiles are clearly present (Figure 4). Izotov & Thuan (2009a) study the galaxy with archival UVES spectroscopy on the Very

Large Telescope taken in 2002 November. These authors conclude the spectral features are due to an LBV, which is reiterated in Izotov et al. (2011) with UV/optical and near-infrared X-SHOOTER spectroscopy obtained in 2009 August (60.A-9442(A), P.I. Diaz). Terlevich et al. (2014) note the presence of Fe II multiplet 42 and infrared Ca II triplet absorption lines blueshifted by the same velocity as the P Cygni absorption. They also obtained ISIS spectroscopy with the William Herschel Telescope in 2011 November and note no significant change in the broad emission between any of the spectra. We show both the SDSS and X-SHOOTER spectra in Figure 4 for comparison with our newly obtained GMOS-N spectrum. Our analysis of the SDSS spectrum  $H\alpha$ -[N II] complex is shown in Figure 3.

We fit a blue power-law continuum of  $f_\lambda \sim 6.4 \times 10^{-17}$  ( $4.0 \times 10^{-17}$ )  $\text{erg s}^{-1} \text{cm}^{-2} \text{\AA}^{-1}$  at 6500  $\text{\AA}$  with index  $-3.1$  ( $-5.0$ ) and reddening of  $f_\lambda \sim 5.2 \times 10^{-17}$  ( $2.8 \times 10^{-17}$ )  $\text{erg s}^{-1} \text{cm}^{-2} \text{\AA}^{-1}$  at 6500  $\text{\AA}$  in the SDSS (Gemini) spectrum.

In the Gemini spectrum, the broad and narrow  $H\alpha$  luminosity is  $2.6 \times 10^{38}$  and  $2.8 \times 10^{39}$   $\text{erg s}^{-1}$ , respectively. In the earlier SDSS spectrum, the broad and narrow  $H\alpha$  luminosity is  $1.3 \times 10^{39}$  and  $3.2 \times 10^{39}$   $\text{erg s}^{-1}$ , respectively. That is, a broad to narrow  $H\alpha$  ratio of 0.41 with SDSS and 0.10 today with Gemini. The ratio of broad to narrow  $H\alpha$  FWHM is 8.5 in the SDSS fitting versus 5.9 in the Gemini fitting. The narrow absorption component is blueshifted by  $807 \pm 65 \text{ km s}^{-1}$  relative to  $H\alpha$  in our model. The broad emission component in the Gemini spectrum is redshifted by  $88 \pm 65 \text{ km s}^{-1}$  relative to  $H\alpha$ . A P Cygni-like absorption feature is clearly present in the earlier SDSS (2001) and X-SHOOTER (2009) spectra. The absorption feature is not clearly visible in Gemini data; therefore, no absorption component was used in our Gemini spectral fitting.

Given the seeing of  $0''.65$  and the  $0''.75$  slit width, a decrease of 17% is expected with respect to the same source observed with an SDSS fiber, assuming the emission is dominated by a Gaussian point source. We indeed measured a decrease in the narrow line flux of 14% compared to the larger  $3''$  SDSS fiber. Variations in the narrow lines, therefore, are due to instrument/aperture effects. We measured a decrease in the broad  $H\alpha$  of 80%. If 14% can be attributed to systematics from the aperture differences, the broad  $H\alpha$  still decreased by about 66%. In addition, both the X-SHOOTER and ISIS spectra used a slit

**Table 1**  
Source Properties and Possible Scenarios

Source Property (1)	LBV Outburst (2)	Stellar Wind (3)	AGN (4)	SN IIn (5)	TDE (6)
Broad emission lines ( $L_{H\alpha} \sim 10^{39}$ erg s $^{-1}$ )	unusually large	YES	YES	YES	unusually low
Decade long-lived broad emission	unusual	YES	YES	unusual	NO
Recent dissipation of broad emission	YES	NO	NO	YES	YES
P Cygni-like profile	YES	YES	unusual	YES	NO
Fe II absorption lines	YES	YES	unusual	YES	NO
800 km s $^{-1}$ blueshift of absorption lines	unusually high	NO	YES	YES	NO
Lack of X-rays ( $\lesssim 2.2 \times 10^{38}$ erg s $^{-1}$ )	YES	YES	NO	unusual	YES
Lack of high-ionization lines ( $\lesssim 120$ eV)	YES	YES	unusual	YES	YES
Small-amplitude optical variability	unusually small	NO	YES	YES	unusually low

**Note.** YES: the observational feature can be readily explained by the proposed scenario. NO: cannot be explained without invoking an exotic or contrived scenario. Unusual: can be explained but it is unusual of observed systems.

width of 1" and the broad emission features were found to be unchanged with SDSS (Izotov et al. 2011; Terlevich et al. 2014). An 80% decrease could be explained if the broad emission is offset by 0".61 from the slit center, inconsistent with Figure 2 (c) which shows the variable source is well-covered by the slit configuration.

Our Gemini spectrum does not cover the Fe II absorption lines; therefore, we cannot determine if the Fe II absorption has weakened or disappeared. Recently, Allan et al. (2020) also report the fading of the broad Balmer emission and disappearance of the P Cygni absorption using new X-SHOOTER spectroscopy taken in 2019 December.

Terlevich et al. (2014) model the H $\alpha$  emission with two broad emission components (one central and one redshifted extremely broad wing) and one narrow blueshifted absorption component. The ultra-broad red wing is no longer present in the Gemini data. A fading ultra-broad red wing was also seen in SDSS1133 (Koss et al. 2014).

Inspection of archival Hubble Space Telescope Cosmic Origins Spectrograph far-UV spectrum shows C III  $\lambda$ 1909 and C IV  $\lambda$ 1549 lines clearly present along with geocoronal Ly- $\alpha$  and O I/Si II.

### 3.1.3. X-Ray

PHL 293B was not detected in 2009 with a 7.7 ks Chandra exposure. The upper limit on the X-ray luminosity is  $\sim 2.2 \times 10^{38}$  erg s $^{-1}$ . In the AGN scenario, this implies an Eddington ratio below  $10^{-5}$  assuming  $M_{\bullet} = 10^5 M_{\odot}$ .

### 3.1.4. Radio

There is no detection in NVSS (1993), FIRST (2002), or VLASS images. From the VLASS sensitivity, we derive an upper limit of the 5 GHz radio luminosity of  $\nu L_{\nu} \sim 4 \times 10^{35}$  erg s $^{-1}$  (assuming a flat spectral index).

## 3.2. Conflicting Interpretations and Likely Scenarios

To understand the nature of PHL 293B, we investigate the following possible scenarios: (a) low-mass AGN driven by a massive black hole, (b) young stellar wind, (c) tidal disruption event, (d) luminous blue variable (LBV) star outburst, or (e) long-lived SN IIn observed at late times. In Table 1, we summarize the major observational properties of PHL 293B and evaluate each scenario. Scenarios (a) and (b) are unlikely given the recent fading of broad H $\alpha$  emission.

The origin of the narrow emission lines is likely the H II region ionized primarily by stellar emission from the massive star cluster. The observed continuum variability of  $\sim 10\%$  implies that most of the continuum originates from the cluster and nebular region. The presence of the high-velocity Fe II absorption implies a relatively cool medium in front of the continuum source, both extended by tens of parsecs. Therefore, the Fe II absorption should also be extended by at least several tens of parsecs, implying a shell or LBV wind expanding at  $\sim 800$  km s $^{-1}$ .

The fading of the light curve and broad emission is unusual for nontransient phenomena such as a stellar wind. This challenges the interpretation of Terlevich et al. (2014) of a superwind driven by a young stellar wind. Also, Tenorio-Tagle et al. (2015) point out that the dynamical time of an expanding shell with speed 800 km s $^{-1}$  would put the shock well outside of the galaxy given the age of the star cluster. Our observations also warrant a more skeptical look at the strongly radiative stationary cooling wind, possibly driven by old supernova remnants, as proposed by Tenorio-Tagle et al. (2015). While many observational features of PHL 293B can be explained by these scenarios, these authors assume no strong photometric or spectral variability in their models.

A tidal disruption event would also be highly unusual given the P Cygni absorption and unusually long-lived broad emission and small-amplitude photometric variability. Furthermore, the broad line width of  $\sim 1500$  km s $^{-1}$  is several times smaller than expected for a typical tidal disruption event (Arcavi et al. 2014).

The optical and spectroscopic variability could arise from two different mechanisms (e.g., the optical variability could be purely stellar in origin with the P Cygni-like feature arising from another source). However, in this Letter we restrict ourselves to the simplest single mechanism which most likely explains all the observed features. Therefore, we argue the nature of the spectral features and variability of PHL 293B is due to a long-lived transient event. We devote the remainder of this section to investigating the remaining likely scenarios of an LBV outburst or long-lived SN IIn.

### 3.2.1. Luminous Blue Variable Star Outburst

LBVs are massive stars in a critical phase in stellar evolution located in the upper-left of the  $H-R$  diagram (Humphreys & Davidson 1994). Every star more massive than about  $50 M_{\odot}$  will go through the LBV phase. Therefore, LBVs should be

more common in BCD galaxies because the high star formation rates and low metallicities enable formation of massive stars.

Izotov & Thuan (2009a) and Izotov et al. (2011) argue that the P Cygni-like spectral features of PHL 293B are evidence for an LBV in its star-forming region. Many of the spectral features observed in PHL 293B such as broad emission, narrow blueshifted absorption lines, and Fe II multiplet and Ca II infrared triplet lines are seen in LBV spectra (Munari et al. 2009; Humphreys et al. 2017). These features can often be seen in the long and fainter quiescent S Doradus phases. However, this seems inconsistent with the high luminosity of the LBV of  $2.5\text{--}5.0 \times 10^6 L_{\odot}$  found by Allan et al. (2020).

In addition, Terlevich et al. (2014) argue that the properties of PHL 293B are unusual of observed LBVs. The  $800 \text{ km s}^{-1}$  blueshifted terminal velocity would be the largest ever reported for an LBV (with  $\eta$  Carinae at  $\sim 500 \text{ km s}^{-1}$ ; Leitherer et al. 1994). These differences are attributed to the LBV undergoing a strong outburst and to effects at very low metallicity by Izotov & Thuan (2009a). However, this is not consistent with the lower blueshifted absorption velocities of LBVs in the two low-metallicity dwarf galaxies NGC 2366 ( $\sim 250 \text{ km s}^{-1}$ ; Drissen et al. 1997) and IC 1613 ( $\sim 300 \text{ km s}^{-1}$ ; Herrero et al. 2010).

Izotov et al. (2011) also note broad  $H\alpha$  luminosity of PHL 293B of  $\sim 10^{39} \text{ erg s}^{-1}$  from 2001 to 2009 is about 10 times greater than the LBV in NGC 2366 (Petit et al. 2006) when corrected for extinction. They conclude the LBV in PHL 293B must therefore be among the most luminous known and undergoing a strong outburst. However, the lack of any large photometric variability in any of the photometric epochs dating back to 1949 is challenging to this scenario.

LBVs, even in extragalactic settings, typically exhibit baseline variability of roughly 1 mag or larger on decade timescales, with sporadic and unpredictable eruptions observed in many cases (Walborn et al. 2017). In particular, P Cygni and  $\eta$  Carinae have undergone massive outbursts of several magnitudes in recorded history. Although a short outburst may have been missed by the photometric gaps in PHL 293B, LBVs should continue to exhibit both photometric variability greater than 0.1 mag even after an outburst (e.g., Smith & Frew 2011). Although long-term trends at this level have been observed in some LBVs, there is no evidence of the expected variability on shorter timescales in PHL 293B. In addition, demonstrable variability of spectral features during or shortly after an eruption should be observed (e.g., Petit et al. 2006; Richardson et al. 2011). Any LBV in a relatively quiescent state that might explain the low-level of photometric variability in PHL 293B is difficult to reconcile with the long-lived broad emission lines and high terminal speed of the shock.

Allan et al. (2020) conclude the LBV is exiting its eruptive phase, is becoming obscured, or has collapsed directly into a black hole without producing a bright SN. The authors do not comment on Fe II absorption line variability. We expect these absorption features to be gone too if the shell of the ejecta has expanded considerably or if the LBV has disappeared or become obscured.

### 3.2.2. Long-lived Type II<sub>n</sub> Supernova

If the features of PHL 293B are due to an evolving young SN remnant, it falls into the rare Type II<sub>n</sub> class. That is, a core-collapse SN with broad and narrow Balmer lines (Schlegel 1990; Filippenko 1997). P Cygni-like narrow absorption lines

are commonly observed in SNe II<sub>n</sub> (e.g., Salamanca et al. 2002). The spectral features are due to the ejecta from a massive progenitor star interacting with the circumstellar medium. There is evidence that this scenario arises when a strong mass loss from an LBV-like progenitor undergoes sustained interaction with a dense circumstellar medium (e.g., Koss et al. 2014; Smith et al. 2017 and references within).

Some Type I and II SNe show high-velocity blueshifted Fe II lines (e.g., Chugai et al. 2004; Smith et al. 2010; Young et al. 2010) and infrared Ca II triplet lines (e.g., Taddia et al. 2013). Missing associated Fe II/Ca II emission lines could be due to an asymmetric explosion, or the emission lines could be very weak and broad at late times making them difficult to detect. The  $800 \text{ km s}^{-1}$  blueshift of the absorption features in PHL 293B's spectrum is not unusual for an expanding envelope of SN II<sub>n</sub> ejecta which can exceed  $1000 \text{ km s}^{-1}$  in some cases (e.g., SN 2009ip; Foley et al. 2011; Smith et al. 2014), but is anomalously high for an LBV wind. Furthermore, the broad emission width in the SDSS and X-SHOOTER spectra of FWHM  $\sim 10^3 \text{ km s}^{-1}$  is not unusual (e.g., Nyholm et al. 2017). Sustaining broad emission of  $10^{39} \text{ erg s}^{-1}$  over 15 yr requires an energy of  $\sim 5 \times 10^{47} \text{ ergs}$ , well below the canonical SN kinetic energy budget of  $10^{51} \text{ ergs}$ .

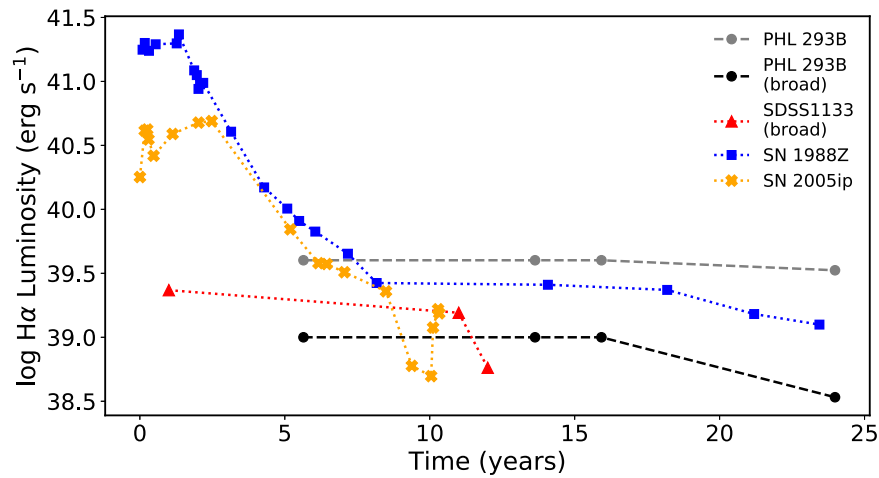
A remarkably similar transient known as SDSS1133 was discovered by Koss et al. (2014) in the BCD galaxy Mrk 177. Like PHL 293B, its broad emission persists for over a decade with broad  $L_{H\alpha} \sim 7 \times 10^{39} \text{ erg s}^{-1}$  at day 4000. SDSS1133 also showed an ultra-broad  $H\alpha$  emission. A growing number of bona fide SNe II<sub>n</sub> are known to display broad emission that persists for a decade or longer. We show the broad  $H\alpha$  luminosity versus time in Figure 5 in comparison with the long-lived SNe II<sub>n</sub> SDSS1133, SN 1988Z, and SN 2005ip (Aretxaga et al. 1999a). The SDSS spectra of SDSS1133 and PHL 293B are shown for comparison in Appendix B.

It is possible the SN II<sub>n</sub>-like event occurred sometime between September 1995 and September 1998 when no photometry is available. In some cases, SNe II<sub>n</sub> light curves exhibit “bumps” several years after the explosion (e.g., Nyholm et al. 2017).

The VLASS upper limit implies the transient is not radio-loud like some very luminous SNe (Smith et al. 2017). In the case of SDSS1133, *Swift* detected X-ray emission with an estimated X-ray luminosity of  $1.5 \times 10^{39} \text{ erg s}^{-1}$  12 yr after the SN (Koss et al. 2014). The X-ray upper limit of PHL 293B of  $2.2 \times 10^{38} \text{ erg s}^{-1}$  in 2009 is an order of magnitude less than SDSS1133. Assuming the SN in PHL 293B took place in 1996, it was observed with Chandra  $\sim 13$  yr after its outburst. SN II<sub>n</sub> generally emit X-rays above a few  $10^{38} \text{ erg s}^{-1}$  even several years after the SN (e.g., Bregman & Pildis 1992); however, their X-ray emission is very diverse and may approach the X-ray limit of PHL 293B 13 yr after the outburst (see Figure 3 of Dwarkadas & Gruszko 2012). This perhaps indicates the outburst in PHL 293B was nonterminal or the X-ray emission has declined steeply at late times.

## 4. Conclusions

The most plausible explanations for the recent dissipation of the broad emission after an unusually persistent phase are an LBV outburst followed by a slow, weakly variable phase or a very long-lived SN II<sub>n</sub> event. The latter is more likely given the lack of short-timescale variability and the slowly fading light curve. The similarity to the persistent transient of Koss et al. (2014) in a



**Figure 5.**  $H\alpha$  luminosity vs. time. SDSS1133 (Koss et al. 2014), SN 1988Z (Aretxaga et al. 1999a; Smith et al. 2017), and SN 2005ip (Smith et al. 2009, 2017) are shown for comparison. The measurement refers to the total  $H\alpha$  luminosity if not specified. We assume the SN in PHL 293B took place on 1996 January 1. The data for PHL 293B prior to this work are estimated as  $10^{39}$   $\text{erg s}^{-1}$  (Izotov & Thuan 2009a; Izotov et al. 2011; Terlevich et al. 2014; whose measurements vary depending on how the broad emission is modeled, but are all consistent with  $10^{39}$   $\text{erg s}^{-1}$ ). The UVES measurement was taken in nonphotometric conditions and is therefore omitted. Uncertainties are dominated by systematic uncertainties, which are difficult to quantify exactly, but are typically  $\pm 20\%$ .

similar BCD galaxy is of note. In this case, the SN occurred sometime between 1988 and 1998 and continued to slowly evolve until today. However, in our case, the evidence for an LBV progenitor is only circumstantial.

The question, “why are there not more dwarf starburst galaxies with broad emission as strong as PHL 293B?” is raised when considering the stationary wind scenario. The unusual nature of PHL 293B and SDSS1133 can be well-understood if they are due to rare stellar transient phenomena. However, high-resolution spectroscopic observations should be conducted in coming years to study its spectral behavior in detail.

We reiterate the warning of Filippenko (1989) that the long-lived spectral features seen of some SNe II can be AGN impostors. This is the case especially at late times when the features are due to ejecta-circumstellar medium interaction as well as SNe at low bolometric luminosities. We extend this warning to low-mass AGN, noting that late-time SN variability can mimic AGN-like variability (also see Aretxaga et al. 1997, 1999b). Perhaps the dense circumstellar medium of metal-poor massive stars plays an important role in extending the lifetime of the broad emission. Izotov & Thuan (2008) and Izotov et al. (2010) identified a handful of low-metallicity compact emission-line galaxies with persistent broad  $H\alpha$  emission. They suggested these systems could be low-mass AGNs. However, no characteristic hard X-ray emission was seen in Chandra images (Simmonds et al. 2016; Baldassare et al. 2017). If the sample of Izotov & Thuan (2008, 2009b), Izotov et al. (2010), Koss et al. (2014), and PHL 293B can be explained by similar mechanisms, then perhaps such long-lived transients are more common in low-metallicity dwarf galaxies. However, the  $H\alpha$  luminosity of the Izotov & Thuan (2008) sample is much larger than PHL 293B. In these scenarios, only follow-up spectroscopy on decade-long or greater timescales can be definitive.

Analysis of difference imaging light curves with the Legacy Survey of Space and Time at Vera C. Rubin Observatory would determine if the source continues to exhibit low-levels of variability or not. We expect little or no continued variability if the SN was terminal. However, we expect continued small-amplitude variability if the progenitor is still present.

We thank Yuri Izotov for helpful correspondence. We thank Tom Diehl and Chris Lidman for helpful comments. C.J.B. is grateful to Kedar Phadke and Gautham Narayan for useful discussion, and to the Illinois Graduate Survey Science Fellowship for support. We thank the referee, Roberto Terlevich, for useful comments and corrections which improved this work.

This research has made use of the NASA/IPAC Extragalactic Database (NED), which is operated by the Jet Propulsion Laboratory, California Institute of Technology, under contract with the National Aeronautics and Space Administration.

Based on observations obtained at the Gemini Observatory, which is operated by the Association of Universities for Research in Astronomy, Inc., under a cooperative agreement with the NSF on behalf of the Gemini partnership: the National Science Foundation (United States), National Research Council (Canada), CONICYT (Chile), Ministerio de Ciencia, Tecnología e Innovación Productiva (Argentina), Ministério da Ciência, Tecnologia e Inovação (Brazil), and Korea Astronomy and Space Science Institute (Republic of Korea).

Support for V.F.B. was provided by the National Aeronautics and Space Administration through Einstein Postdoctoral Fellowship Award Number PF7-180161 issued by the Chandra X-ray Observatory Center, which is operated by the Smithsonian Astrophysical Observatory for and on behalf of the National Aeronautics Space Administration under contract NAS8-03060.

Funding for the Sloan Digital Sky Survey IV has been provided by the Alfred P. Sloan Foundation, the U.S. Department of Energy Office of Science, and the Participating Institutions. SDSS-IV acknowledges support and resources from the Center for High-Performance Computing at the University of Utah. The SDSS website is [www.sdss.org](http://www.sdss.org).

SDSS-IV is managed by the Astrophysical Research Consortium for the Participating Institutions of the SDSS Collaboration including the Brazilian Participation Group, the Carnegie Institution for Science, Carnegie Mellon University, the Chilean Participation Group, the French Participation Group, Harvard-Smithsonian Center for Astrophysics, Instituto de Astrofísica de Canarias, The Johns Hopkins University,



Kavli Institute for the Physics and Mathematics of the Universe (IPMU)/University of Tokyo, the Korean Participation Group, Lawrence Berkeley National Laboratory, Leibniz Institut für Astrophysik Potsdam (AIP), Max-Planck-Institut für Astronomie (MPIA Heidelberg), Max-Planck-Institut für Astrophysik (MPA Garching), Max-Planck-Institut für Extraterrestrische Physik (MPE), National Astronomical Observatories of China, New Mexico State University, New York University, University of Notre Dame, Observatório Nacional / MCTI, The Ohio State University, Pennsylvania State University, Shanghai Astronomical Observatory, United Kingdom Participation Group, Universidad Nacional Autónoma de México, University of Arizona, University of Colorado Boulder, University of Oxford, University of Portsmouth, University of Utah, University of Virginia, University of Washington, University of Wisconsin, Vanderbilt University, and Yale University.

Funding for the DES Projects has been provided by the U.S. Department of Energy, the U.S. National Science Foundation, the Ministry of Science and Education of Spain, the Science and Technology Facilities Council of the United Kingdom, the Higher Education Funding Council for England, the National Center for Supercomputing Applications at the University of Illinois at Urbana-Champaign, the Kavli Institute of Cosmological Physics at the University of Chicago, the Center for Cosmology and Astro-Particle Physics at the Ohio State University, the Mitchell Institute for Fundamental Physics and Astronomy at Texas A&M University, Financiadora de Estudos e Projetos, Fundação Carlos Chagas Filho de Amparo à Pesquisa do Estado do Rio de Janeiro, Conselho Nacional de Desenvolvimento Científico e Tecnológico and the Ministério da Ciência, Tecnologia e Inovação, the Deutsche Forschungsgemeinschaft and the Collaborating Institutions in the Dark Energy Survey.

The Collaborating Institutions are Argonne National Laboratory, the University of California at Santa Cruz, the University of Cambridge, Centro de Investigaciones Energéticas, Medioambientales y Tecnológicas-Madrid, the University of Chicago, University College London, the DES-Brazil Consortium, the University of Edinburgh, the Eidgenössische Technische Hochschule (ETH) Zürich, Fermi National Accelerator Laboratory, the University of Illinois at Urbana-Champaign, the Institut de Ciències de l'Espai (IEEC/CSIC), the Institut de Física d'Altes Energies, Lawrence Berkeley National Laboratory, the Ludwig-Maximilians Universität München and the associated Excellence Cluster Universe, the University of Michigan, the National Optical Astronomy Observatory, the University of Nottingham, The Ohio State University, the University of Pennsylvania, the University of Portsmouth, SLAC National Accelerator Laboratory, Stanford University, the University of Sussex, Texas A&M University, and the OzDES Membership Consortium.

Based in part on observations at Cerro Tololo Inter-American Observatory, National Optical Astronomy Observatory, which is operated by the Association of Universities for Research in Astronomy (AURA) under a cooperative agreement with the National Science Foundation.

The DES data management system is supported by the National Science Foundation under grant Nos. AST-1138766 and AST-1536171. The DES participants from Spanish institutions are partially supported by MINECO under grants AYA2015-71825, ESP2015-66861, FPA2015-68048, SEV-2016-0588, SEV-2016-0597, and MDM-2015-0509, some of

which include ERDF funds from the European Union. IFAE is partially funded by the CERCA program of the Generalitat de Catalunya. Research leading to these results has received funding from the European Research Council under the European Union's Seventh Framework Program (FP7/2007–2013) including ERC grant agreements 240672, 291329, and 306478. We acknowledge support from the Brazilian Instituto Nacional de Ciência e Tecnologia (INCT) e-Universe (CNPq grant 465376/2014-2).

This manuscript has been authored by Fermi Research Alliance, LLC under Contract No. DE-AC02-07CH11359 with the U.S. Department of Energy, Office of Science, Office of High Energy Physics.

*Facilities:* SDSS, Blanco Gemini(GMOS-N).

*Software:* astropy, hotpants, PyQSOFit.

## Appendix A Light-curve Construction and Analysis

Difference imaging was performed independently on SDSS and DES data. The SDSS pipeline described in Baldassare et al. (2018) makes use of a modified version of the Difference Imaging and Analysis Pipeline 2 (Wozniak 2000). The DES difference pipeline is described in Kessler et al. (2015) and is based on HOTPANTS (Becker 2017). Both codes rely on the basic image subtraction algorithm described in Alard & Lupton (1998) and Alard (2000). Our procedure for constructing our DIA light curves is as follows: We construct a template image using single-epoch frames with the best seeing and lowest background. Next, we convolve each image with a kernel function to approximately match the PSF in the DES template image. Then we subtract the convolved single-epoch image from the template to create the difference image. Finally, we perform aperture photometry on the difference image within a  $2''.5$  radius circle centered on the target galaxy nucleus.

We invoke the CARMA\_PACK software (Kelly et al. 2018) to perform a Markov chain Monte Carlo fitting to a DRW model. In the framework of Kelly et al. (2014), the standard DRW model is the continuous-time first-order autoregressive (CAR(1)) Gaussian process. To assess the fit, we calculate  $[\chi^2/\nu]_{\text{DRW}}$  from the standardized residuals of the DRW/CAR(1) model, assuming the number of degrees of freedom is  $N-2$  (for the two parameters in the CAR(1) process).

We also calculate the standard variability metric  $[\chi^2/\nu]_{\text{var}}$ :

$$[\chi^2/\nu]_{\text{var}} = \frac{1}{\nu} \sum_{i=1}^N (m_i - \bar{m})^2 w_i \quad (\text{A1})$$

where the weighted mean  $\bar{m}$  is given by,

$$\bar{m} = \frac{\sum_{i=1}^N m_i w_i}{\sum_{i=1}^N w_i}, \quad (\text{A2})$$

with weights given by the reciprocal of the photometric errors  $w_i = 1/\sigma_i^2$  on each measurement  $m_i$  (in magnitudes). We then calculate the resulting significance  $\sigma_{\text{var}}$  from the  $\chi^2$  distribution in units of  $\sigma$ . We find significant variability with  $\sigma_{\text{var}} > 3$  in both SDSS and DES  $g$  and  $r$  band light curves for PHL 293B before combining the photometry.

## Appendix B Comparison of Spectra to SDSS1133

For comparison, we show the SDSS spectra of PHL 293B and SDSS1133 in Figure B1.

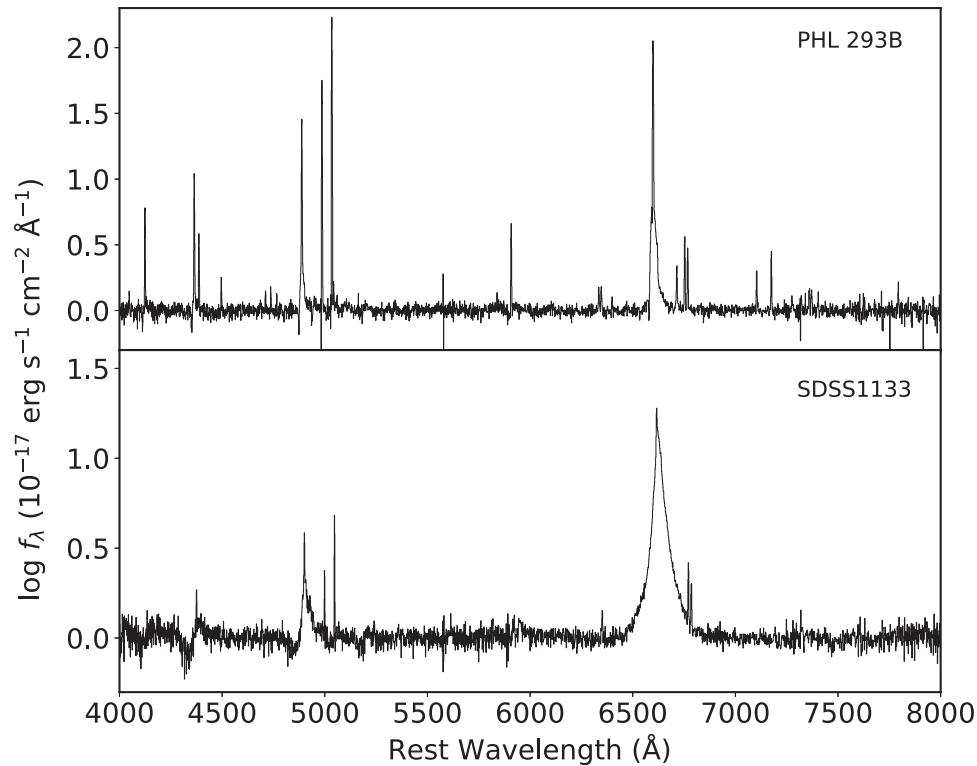


Figure B1. Comparison of SDSS spectra of PHL 293B and SDSS1133.

### ORCID iDs

Colin J. Burke <https://orcid.org/0000-0001-9947-6911>  
 Vivienne F. Baldassare <https://orcid.org/0000-0003-4703-7276>  
 Xin Liu <https://orcid.org/0000-0003-0049-5210>  
 Yue Shen <https://orcid.org/0000-0003-1659-7035>  
 Antonella Palmese <https://orcid.org/0000-0002-6011-0530>  
 Hengxiao Guo <https://orcid.org/0000-0001-8416-7059>  
 David Brooks <https://orcid.org/0000-0002-8458-5047>  
 Matias Carrasco Kind <https://orcid.org/0000-0002-4802-3194>  
 Juan García-Bellido <https://orcid.org/0000-0002-9370-8360>  
 Daniel Gruen <https://orcid.org/0000-0003-3270-7644>  
 Robert A. Gruendl <https://orcid.org/0000-0002-4588-6517>  
 Devon L. Hollowood <https://orcid.org/0000-0002-9369-4157>  
 Kyler Kuehn <https://orcid.org/0000-0003-0120-0808>  
 Ramon Miquel <https://orcid.org/0000-0002-6610-4836>  
 Eusebio Sanchez <https://orcid.org/0000-0002-9646-8198>  
 Marcelle Soares-Santos <https://orcid.org/0000-0001-6082-8529>  
 Molly E. C. Swanson <https://orcid.org/0000-0002-1488-8552>  
 Gregory Tarle <https://orcid.org/0000-0003-1704-0781>  
 Alistair R. Walker <https://orcid.org/0000-0002-7123-8943>

### References

- Alard, C. 2000, *A&AS*, 144, 363  
 Alard, C., & Lupton, R. H. 1998, *ApJ*, 503, 325  
 Allan, A., Groh, J., Mehner, A., et al. 2020, arXiv:2003.02242  
 Arcavi, I., Gal-Yam, A., Sullivan, M., et al. 2014, *ApJ*, 793, 38  
 Arétxaga, I., Benetti, S., Terlevich, R. J., et al. 1999a, *MNRAS*, 309, 343  
 Arétxaga, I., Fernandes Roberto Cid, J., & Terlevich, R. J. 1997, *MNRAS*, 286, 271  
 Arétxaga, I., Jöguet, B., Kunth, D., Melnick, J., & Terlevich, R. J. 1999b, *ApJL*, 519, L123  
 Baldassare, V. F., Geha, M., & Greene, J. 2018, *ApJ*, 868, 152  
 Baldassare, V. F., Reines, A. E., Gallo, E., & Greene, J. E. 2017, *ApJ*, 836, 20  
 Becker, A. C. 2017, hotpants, <https://github.com/acbecker/hotpants>  
 Bregman, J. N., & Pildis, R. A. 1992, *ApJL*, 398, L107  
 Cairós, L. M., Vílchez, J. M., González Pérez, J. N., Iglesias-Páramo, J., & Caon, N. 2001, *ApJS*, 133, 321  
 Chugai, N. N., Blinnikov, S. I., Cumming, R. J., et al. 2004, *MNRAS*, 352, 1213  
 Dark Energy Survey Collaboration 2016, *MNRAS*, 460, 1270  
 Drissen, L., Roy, J.-R., & Robert, C. 1997, *ApJL*, 474, L35  
 Drlica-Wagner, A., Sevilla-Noarbe, I., Rykoff, E. S., et al. 2018, *ApJS*, 235, 33  
 Dwarkadas, V. V., & Gruszko, J. 2012, *MNRAS*, 419, 1515  
 Filippenko, A. V. 1989, *AJ*, 97, 726  
 Filippenko, A. V. 1997, *ARA&A*, 35, 309  
 Flaugher, B., Diehl, H. T., Honscheid, K., et al. 2015, *AJ*, 150, 150  
 Foley, R. J., Berger, E., Fox, O., et al. 2011, *ApJ*, 732, 32  
 French, H. B. 1980, *ApJ*, 240, 41  
 Geha, M., Blanton, M. R., Masjedi, M., & West, A. A. 2006, *ApJ*, 653, 240  
 Guo, H., Shen, Y., & Wang, S. 2018, PyQSOFit: Python code to fit the spectrum of quasars, Astrophysics Source Code Library, version 1.0, ascl:1809.008

- Herrero, A., Garcia, M., Uytterhoeven, K., et al. 2010, *A&A*, **513**, A70
- Humphreys, R. M., & Davidson, K. 1994, *PASP*, **106**, 1025
- Humphreys, R. M., Gordon, M. S., Martin, J. C., Weis, K., & Hahn, D. 2017, *ApJ*, **836**, 64
- Izotov, Y. I., Guseva, N. G., Fricke, K. J., et al. 2010, *A&A*, **517**, A90
- Izotov, Y. I., Guseva, N. G., Fricke, K. J., & Henkel, C. 2011, *A&A*, **533**, A25
- Izotov, Y. I., & Thuan, T. X. 2008, *ApJ*, **687**, 133
- Izotov, Y. I., & Thuan, T. X. 2009a, *ApJ*, **690**, 1797
- Izotov, Y. I., & Thuan, T. X. 2009b, *ApJ*, **707**, 1560
- Kelly, B. C., Bechtold, J., & Siemiginowska, A. 2009, *ApJ*, **698**, 895
- Kelly, B. C., Becker, A. C., Sobolewska, M., Siemiginowska, A., & Uttley, P. 2014, *ApJ*, **788**, 33
- Kelly, B. C. 2018, carma\_pack, [https://github.com/brandonckelly/carma\\_pack](https://github.com/brandonckelly/carma_pack)
- Kessler, R., Marriner, J., Childress, M., et al. 2015, *AJ*, **150**, 172
- Kinman, T. D. 1965, *ApJ*, **142**, 1241
- Koss, M., Blecha, L., Mushotzky, R., et al. 2014, *MNRAS*, **445**, 515
- Leitherer, C., Allen, R., Altner, B., et al. 1994, *ApJ*, **428**, 292
- MacLeod, C. L., Ivezić, Ž., Kochanek, C. S., et al. 2010, *ApJ*, **721**, 1014
- Micheva, G., Östlin, G., Bergvall, N., et al. 2013, *MNRAS*, **431**, 102
- Munari, U., Siviero, A., Bienaymé, O., et al. 2009, *A&A*, **503**, 511
- Nyholm, A., Sollerman, J., Taddia, F., et al. 2017, *A&A*, **605**, A6
- Petit, V., Drissen, L., & Crowther, P. A. 2006, *AJ*, **132**, 1756
- Richardson, N. D., Morrison, N. D., Gies, D. R., et al. 2011, *AJ*, **141**, 120
- Salamanca, I., Terlevich, R. J., & Tenorio-Tagle, G. 2002, *MNRAS*, **330**, 844
- Schlegel, E. M. 1990, *MNRAS*, **244**, 269
- Shen, Y., Hall, P. B., Horne, K., et al. 2019, *ApJS*, **241**, 34
- Simmonds, C., Bauer, F. E., Thuan, T. X., et al. 2016, *A&A*, **596**, A64
- Smith, N., Chornock, R., Silverman, J. M., Filippenko, A. V., & Foley, R. J. 2010, *ApJ*, **709**, 856
- Smith, N., & Frew, D. J. 2011, *MNRAS*, **415**, 2009
- Smith, N., Kilpatrick, C. D., Mauerhan, J. C., et al. 2017, *MNRAS*, **466**, 3021
- Smith, N., Mauerhan, J. C., & Prieto, J. L. 2014, *MNRAS*, **438**, 1191
- Smith, N., Silverman, J. M., Chornock, R., et al. 2009, *ApJ*, **695**, 1334
- Taddia, F., Stritzinger, M. D., Sollerman, J., et al. 2013, *A&A*, **555**, A10
- Tarrab, I. 1987, *A&AS*, **71**, 449
- Tenorio-Tagle, G., Silich, S., Martínez-González, S., Terlevich, R., & Terlevich, E. 2015, *ApJ*, **800**, 131
- Terlevich, R., Terlevich, E., Bosch, G., et al. 2014, *MNRAS*, **445**, 1449
- Thuan, T. X., & Martin, G. E. 1981, *ApJ*, **247**, 823
- Walborn, N. R., Gamen, R. C., Morrell, N. I., et al. 2017, *AJ*, **154**, 15
- Wozniak, P. R. 2000, *AcA*, **50**, 421
- Young, D. R., Smartt, S. J., Valenti, S., et al. 2010, *A&A*, **512**, A70